


 Cite this: *Soft Matter*, 2024, 20, 6539

 Received 28th June 2024,
Accepted 29th July 2024

DOI: 10.1039/d4sm00789a

rsc.li/soft-matter-journal

Azaylide-based gemini amphiphiles displaying unique self-assembling behavior *via* an even–odd effect of alkyl linker chain length†

 Yoshimori Akiyama, Masahiro Yamashina * and Shinji Toyota *

Herein, we report a straightforward synthesis of azaylide-based gemini amphiphiles using bis(diphenylphosphino)alkanes *via* the Staudinger reaction. The prepared gemini amphiphiles exhibited an even–odd effect in their self-assembly behavior depending on the length of the alkyl linkers. Furthermore, the assembled micelles had high host capability toward hydrophobic guests in water.

Gemini amphiphiles consist of two hydrophilic moieties and two hydrophobic moieties connected through a linker.^{1–5} These amphiphiles are generally highly functional compared with their monomeric amphiphiles;^{6–9} therefore, they have been utilized in various applications including drug and gene delivery,^{10–14} antibacterial agents,^{15–18} corrosion inhibitors,^{19,20} phase transfer catalysts,²¹ and microemulsion stabilizers.^{22–24} In terms of the even–odd effect,^{25–28} which is the oscillation in properties depending on the even or odd number of connected repeating units (*e.g.*, methylene group), some gemini amphiphiles comprising aliphatic moieties (*e.g.*, *n*-alkane) as building blocks display a unique self-assembling behavior.^{29–31} Although these examples are based on long alkyl linkers, *e.g.*, (CH₂)_{*n*} with *n* = 10 and 12, the even–odd effect of short alkyl chains can be expected to dramatically change the aggregation behavior owing to their considerable impact on the molecular structure.^{32,33} However, systematic studies on the self-assembly of gemini amphiphiles with short alkyl linkers are scarce.^{31,34} We previously reported the facile transformation of hydrophobic triarylphosphines toward monomeric amphiphiles *via* the Staudinger reaction.^{35,36} The obtained azaylide-based (*i.e.*, N=P bond) amphiphiles self-assembled into *ca.* 2-nm-sized spherical micelles that could encapsulate various hydrophobic dyes in water. In addition to monophosphines, diphosphines such as bis(diphenylphosphino)alkanes with various alkyl chains exhibit different catalytic activities depending on the alkyl chain length and are

commercially available (Fig. 1a).³⁷ In this study, we focused on azaylide-based gemini amphiphiles³⁸ with a short alkyl linkage (**NdpPn**; *n* = 1–6, Fig. 1b) based on bis(diphenylphosphino)alkanes (**dpPn**) as the building blocks and investigated the unique self-assembling behavior of **NdpPn** in water along with that of the corresponding monomeric amphiphile **NPPh2Me** (Fig. 1c and d) for comparison.

A series of azaylide-based gemini amphiphiles were successfully synthesized by simply mixing hydrophilic azide **1** and bis(diphenylphosphino)alkanes in CH₃CN. To prevent residual free hydrophilic azide **1** and intermediates (*e.g.*, monosubstituted product), a small excess of bis(diphenylphosphino)alkanes was added to **1** two times. First, 0.45 equiv. of bis(diphenylphosphino)propane (**dpP3**) was added to a CH₃CN solution of hydrophilic azide **1** (1.0 equiv.) and stirred at 60 °C until complete consumption of **dpP3** (*ca.* 10 min). Subsequently, a CHCl₃ solution of **dpP3** (0.075 equiv.) was slowly added to the resultant solution over 10 min to afford the desired

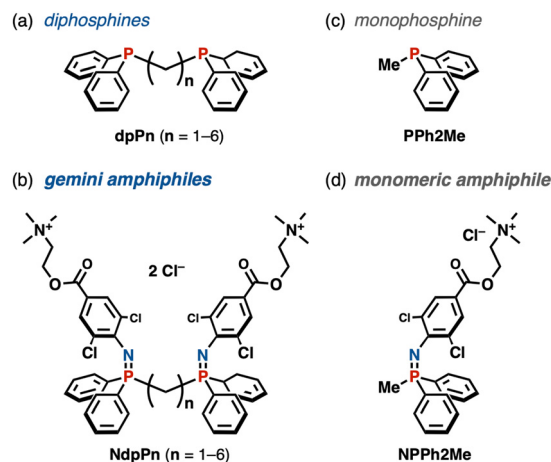


Fig. 1 Chemical structures of (a) diphosphines **dpPn** (*n* = 1–6) and (c) monophosphine **PPh2Me**. (b) Chemical structures of azaylide-based gemini amphiphiles **NdpPn** (*n* = 1–6) and (d) the corresponding monomeric amphiphile **NPPh2Me**.

Department of Chemistry, School of Science, Tokyo Institute of Technology, Meguro-ku, 2-12-1 Ookayama, Tokyo 152-8551, Japan.

E-mail: yamashina@chem.titech.ac.jp, stoyota@chem.titech.ac.jp

† Electronic supplementary information (ESI) available. CCDC 2342817 and 2342818. For ESI and crystallographic data in CIF or other electronic format see DOI: <https://doi.org/10.1039/d4sm00789a>



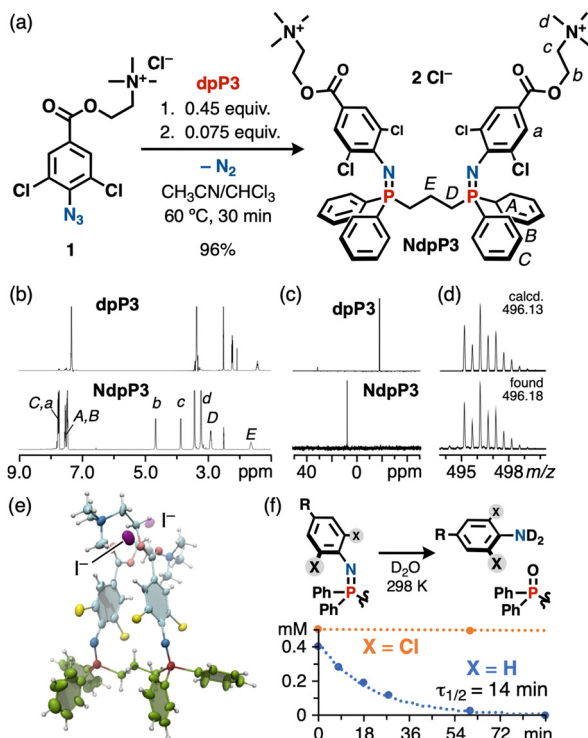


Fig. 2 (a) Synthesis of azaylide-based gemini amphiphile **NdpP3** via the Staudinger reaction. (b) ^1H NMR (500 MHz, $\text{DMSO}-d_6$, 298 K) and (c) ^{31}P NMR (202 MHz, $\text{DMSO}-d_6$, 298 K) spectra of **dpP3** (top) and **NdpP3** (bottom). (d) ESI-TOF MS ($\text{CH}_3\text{CN}/\text{CH}_3\text{OH}$) spectrum of **NdpP3**. (e) X-ray crystal structure of **NdpP3**¹. Thermal ellipsoids are set at 50% probability. (f) Time-course of the decomposition of **NdpP3** and **nNdpP3** in D_2O .

gemini amphiphile **NdpP3** in excellent yield (96%), as confirmed by NMR and MS analyses (Fig. 2a). After the formation of the azaylide ($\text{N}=\text{P}$ bond), a ^{31}P NMR signal attributable to **NdpP3** appeared at 7.3 ppm, which shifted downfield by +25.1 ppm relative to that of free **dpP3**, and the ^1H NMR signals of the **dpP3** moiety showed downfield shift ($\Delta\delta = +0.69$ ppm, Fig. 2b and c). The mass spectrum of dicationic **NdpP3** showed a prominent signal at $m/z = 496.18$ for $[\text{M}-2\text{Cl}]^{2+}$ (Fig. 2d). The other gemini amphiphiles were synthesized in a similar manner in 87–98% yields (Fig. S1, ESI[†]). Interestingly, the synthesis of **NdpP1** required a longer reaction time (3 h), higher concentration (113 mM), and higher temperature (80 °C) due to the increased steric repulsion between the diphenylphosphine moieties. The crowded aromatic rings and phosphine moieties exerted synergistic shielding effects, resulting in a remarkable downfield shift of the ^1H signal of the methylene linker and an upfield shift of the ^{31}P signal compared with those of other **NdpPn**.

A single-crystal X-ray diffraction (SXRD) analysis of **NdpP3**¹, in which the counter ions in **NdpP3** were replaced with two iodide ions, unambiguously revealed the chemical structure of gemini amphiphile **NdpP3** (Fig. 2e and Fig. S2, ESI[†]), which consisted of two hydrophilic parts connected to the **dpP3** moiety in the same direction, *i.e.*, in the *syn*-conformation. One phenyl group of **dpP3** and a phenyl azaylide moiety formed a *trans*-stilbene-like structure.³⁵ **NdpP3** displayed an absorption band ($\lambda_{\text{max}} = 318$ nm) and a weak blue emission ($\lambda_{\text{em}} = 450$ nm)

in CH_3CN (Fig. S4, ESI[†]), similar to those of a previously reported azaylide-based amphiphile with PPh_3 .³⁵ The other azaylide compounds **NdpP1** and **NdpP5** showed excellent water solubility. Non-chlorinated **nNdpP3** was extremely fragile in D_2O , exhibiting a lifetime ($\tau_{1/2}$) of 14 min (Fig. 2f and Fig. S5 and S6, ESI[†]), whereas a triphenylphosphine-based azaylide³⁵ showed a relatively long $\tau_{1/2}$ of 9.8 h. This result indicates that electron-rich yet less sterically hindered alkyl phosphines accelerate the hydrolysis of the azaylide moiety. Nevertheless, chlorinated **NdpP3** exhibited high stability against hydrolysis even in water (Fig. 2f and Fig. S7, ESI[†]). Thus, our strategy can be applied to bis(diphenylphosphino)alkanes with reactive phosphine sites.

Next, the self-assembling behavior of the gemini amphiphiles was investigated in water. First, the amphiphiles with an odd number of methylene linkers, *i.e.*, **NdpP1**, **NdpP3**, and **NdpP5**, were examined. When **NdpP3** was dissolved in D_2O (2.0 mM), (**NdpP3**)_m micelle aggregates were quantitatively and spontaneously formed (Fig. 3a (top)). The ^1H and ^{31}P NMR signals of **NdpP3** in D_2O were substantially broadened owing to the dynamic behavior (Fig. S8 and S9, ESI[†]). A diffusion-ordered spectroscopy (DOSY) analysis revealed a single band at a small diffusion coefficient (D) of $2.28 \times 10^{-10} \text{ m}^2 \text{ s}^{-1}$ (Fig. S20, ESI[†]). According to the Stokes–Einstein equation, this D value corresponds to aggregates with a diameter of *ca.* 1.7 nm. A dynamic light scattering (DLS) analysis revealed the formation of

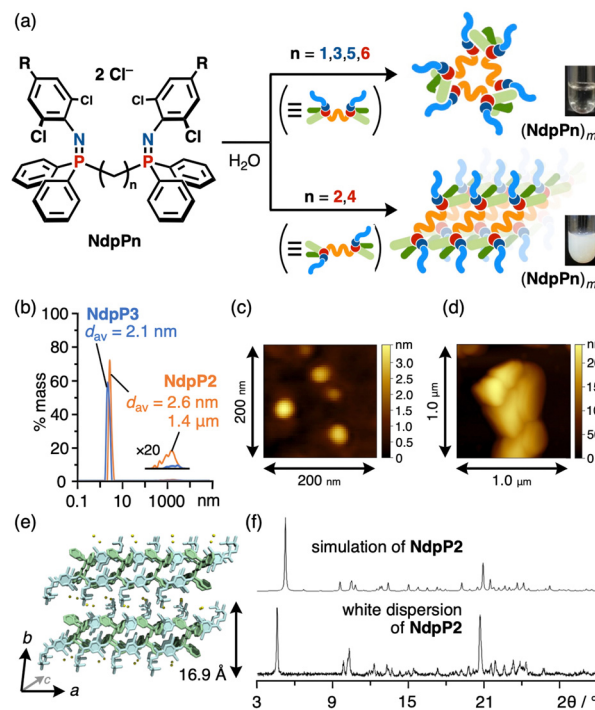


Fig. 3 (a) Schematic of differences in assembling behavior into micelles and layered structures in water. (b) DLS charts of a 2.0 mM aqueous suspension of **NdpP3** and **NdpP2** (298 K). AFM images of (c) micelles of **NdpP3** and (d) the layered structure of **NdpP2**. (e) X-ray packing structure of **NdpP2**. (f) PXRD patterns of a white dispersion of **NdpP2** and simulation based on the results of SXRD of **NdpP2**.



aggregates with a diameter of *ca.* 2.1 nm in water with a narrow size distribution (Fig. 3b and Fig. S21, ESI[†]). Atomic force microscopy (AFM) measurements confirmed the existence of spherical aggregates $(\text{NdpP3})_m$ with a height of *ca.* 2–3 nm (Fig. 3c and Fig. S28, ESI[†]). These results indicate that the size of the $(\text{NdpP3})_m$ micelle aggregates corresponds to four molecules of **NdpP3**, as estimated by molecular mechanics (MM) calculations (Fig. S22, ESI[†]). The critical micelle concentration (CMC) of **NdpP3** was measured using concentration-dependent ¹H NMR and DOSY analyses. The *D* values suddenly decreased when the concentration reached 1.0 mM, which was accompanied by a broadening of the ¹H NMR signals (Fig. S23 and S26, ESI[†]). Thus, the CMC of **NdpP3** was determined to be 1.0 mM, which is considerably lower than that of the monomeric amphiphile **NPPH2Me** (10 mM, Fig. S25, ESI[†]). The other amphiphiles **NdpP1** and **NdpP5** also formed micelle aggregates in water with relatively small CMC values (1.0 and 0.20 mM, respectively, Fig. S10–S13, S20–S22, S24, and S26, ESI[†]). Owing to the increased hydrophobicity, the CMC values gradually decreased with increasing methylene linker length.

Different results were obtained for the amphiphiles with an even number of methylene linkers, *i.e.*, **NdpP2** and **NdpP4**. When **NdpP2** (4.0 μmol) was added to H₂O (2.0 mL), a white suspension was obtained instead of a clear aqueous solution (Fig. 3a (bottom)). A DLS analysis of the suspension revealed the existence of two kinds of aggregates, one type with a diameter of *ca.* 2.6 nm and a narrow distribution and another type with a diameter of *ca.* 1.4 μm and a broadened distribution (Fig. 3b). ¹H NMR analyses showed sharp signals with a large *D* value of $5.25 \times 10^{-10} \text{ m}^2 \text{ s}^{-1}$ at 298 K in water (Fig. S14, S15 and S20, ESI[†]). The fact that **NdpP2** has low water-solubility (*ca.* 0.41 mM) suggests that **NdpP2** is in a monodisperse state or forming premicelles in water. Apart from these **NdpP2**, most of the **NdpP2** molecules formed a white suspension consisting of *ca.* 1–2 μm aggregates in water. AFM and transmission electron microscopy (TEM) observations showed large aggregates (*ca.* 1–2 μm) and spherical small aggregates (*ca.* 3–10 nm), which are consistent with the DLS results (Fig. S28 and S29, ESI[†]). In particular, the AFM image revealed that the large aggregates exhibit a multilayered structure (Fig. 3d), implying the formation of microcrystals.^{39,40}

To gain more insight into the self-assembled structures, X-ray diffraction analyses were conducted. Slow evaporation of a CH₃CN/CHCl₃ solution of **NdpP2** resulted in plate-shaped single crystals, whose SXRD analysis revealed that the two hydrophilic moieties possessed an *anti*-conformation, differing from that of **NdpP3** (Fig. 2e). In the crystalline packing, elongated **NdpP2** molecules were aligned to form a layered structure; specifically, the amphiphiles formed 2D-sheets through multiple CH–π interactions along the *a*- and *c*-axes, and these 2D-sheets stacked in the *b*-axis (Fig. 3e). The powder X-ray diffraction (PXRD) pattern of white dispersions of **NdpP2** in water was consistent with the simulation pattern of **NdpP2** based on the SXRD analysis (Fig. 3f). A similar PXRD pattern was found for **NdpP4** (Fig. S27, ESI[†]). Thus, unlike the micelle formation of **NdpP1**, **NdpP3**, and **NdpP5**, both **NdpP2** and

NdpP4 exhibited high crystallinity with packing structures similar to that shown in Fig. 3e in water. These differences stem most likely from the dipole moments of **NdpP3** (38.66 D) and **NdpP2** (4.84 D), with the latter resulting in a strong packing force.

Contrary to our expectations, **NdpP6** with an even number of methylene linkers was highly soluble in water, resulting in the formation of micelles with a diameter of *ca.* 2–3 nm instead of a layered structure (Fig. S18–S21, ESI[†]). Increasing the length of the alkyl linker chain should endow the gemini amphiphiles with conformational flexibility, leading to the formation of micelle aggregates in water. This observation indicates that the remarkable even–odd effect of the alkyl linker on the assembly behavior is unambiguous for the amphiphiles with short linkers up to *n* = 5.

Finally, the host capability of the gemini amphiphiles was investigated. **NdpP3** (4.0 μmol) and perylene (**Per**; 1.0 equiv.) were ground in a mortar for 3 min, followed by the addition of water (2.0 mL), and the mixture was stirred vigorously for 1 h. After removal of excess guest powders *via* filtration, a yellow solution of $(\text{Per})_x \cdot (\text{NdpP3})_m$ was obtained (Fig. 4a). The UV-vis spectrum clearly displayed absorption bands around 401 nm ascribable to encapsulated hydrophobic **Per** (Fig. 4b). Encapsulated **Per** exhibited weak excimer emission (Fig. S30, ESI[†]). The host–guest complex $(\text{Per})_x \cdot (\text{NdpP3})_m$ was *ca.* 2.7 nm in diameter, as confirmed by DLS measurement (Fig. 4c). The ¹H NMR spectrum of a DMSO-*d*₆ solution of the solid revealed that the amount of encapsulated **Per** was 0.87 mM in 2.0 mM of **NdpP3** aqueous solution (Fig. S36, ESI[†]). Considering these results, MM calculation provided $(\text{Per})_2 \cdot (\text{NdpP3})_5$ as an average host–guest complex model (Fig. 4a (right) and Fig. S39, ESI[†]). Similarly, **NdpP3** successfully encapsulated other hydrophobic

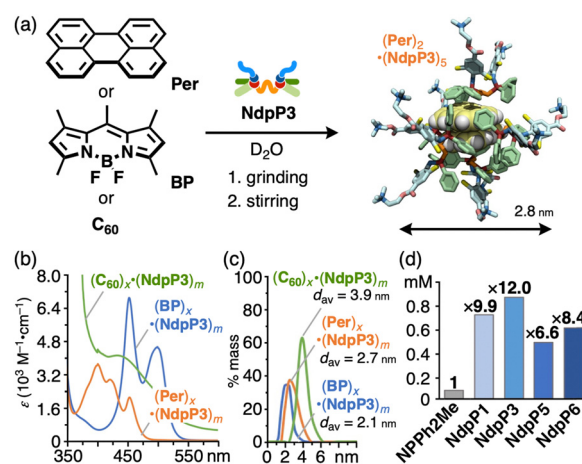


Fig. 4 (a) Schematic of the encapsulation of hydrophobic guests (pyrromethene 546 (BP), perylene (**Per**), and fullerene (C₆₀)) by **NdpP3** in water and the optimized structure of $(\text{Per})_2 \cdot (\text{NdpP3})_5$. (b) UV-vis spectra and (c) DLS charts of $(\text{Per})_x \cdot (\text{NdpP3})_m$, $(\text{BP})_x \cdot (\text{NdpP3})_m$, and $(\text{C}_{60})_x \cdot (\text{NdpP3})_m$ (H₂O, 298 K, 2.0 mM based on **NdpP3**). (d) Comparisons of the uptake quantity of **Per** by **NPPH2Me** and **NdpPn** (*n* = 1, 3, 5, 6). The numbers above the bars indicate relative uptake ratio to **NPPH2Me** (note: **NPPH2Me** was used 4.0 mM to unify the concentration of diphenylphosphino moiety).



guests such as pyromethene 546 (**BP**) and fullerene (**C60**) in water (Fig. 4a and Fig. S30–S39, ESI†). It should be noted that the guest uptake ability of gemini amphiphile **NdpP3** toward **Per** was much higher than that of the monomeric amphiphile **NPPh2Me** (0.072 mM, Fig. 4d). Interestingly, the host capability toward **Per** of the other gemini amphiphiles, *i.e.*, **NdpP1**, **NdpP5**, and **NdpP6**, was similar regardless of the length of the alkyl linker (Fig. 4d and Fig. S30, S33, S36, S39, ESI†). This tendency was observed in the case of **BP** (Fig. S37 and S38, ESI†). Considering that aromatic moieties can effectively encapsulate guest molecules in water,^{9,35,36,41} the bound hydrophobic cores may play a key role in the effective molecular encapsulation.

In conclusion, we have successfully synthesized a series of azaylide-based gemini amphiphiles from bis(diphenylphosphino) alkanes *via* the Staudinger reaction. The gemini amphiphiles exhibited an even–odd effect of the alkyl chain length on their assembly behavior. Our findings provide useful guidance for designing new types of multilinked amphiphiles (*e.g.* gemini and bola⁴¹ amphiphiles) in the near future.

This study was supported by a JSPS Grant-in-Aid for Scientific Research (20H02721), Grants-in-Aid for Early-Career Scientists (22K14662), and the Cooperative Research Program of “NJRC Mater. & Dev. (MEXT).” The authors thank Tokyo Tech. Open Facility Center. The X-ray analysis was performed under the approval of the Photon Factory Program Advisory Committee (2021G046, PF-BL5a). We appreciate Prof. Masaki Kawano (Tokyo Tech.) for X-ray analysis and Prof. Kei Goto (Tokyo Tech.) for the FTIR measurements. We also appreciate valuable discussions with Dr Eiji Tsurumaki (Tokyo Tech.).

Data availability

The data underlying this study are available in the published article and its ESI.†

Conflicts of interest

There are no conflicts to declare.

Notes and references

- 1 F. M. Menger and C. A. Littau, *J. Am. Chem. Soc.*, 1991, **113**, 1451–1452.
- 2 F. M. Menger and J. S. Keiper, *Angew. Chem., Int. Ed.*, 2000, **39**, 1906–1920.
- 3 R. Zana, *Adv. Colloid Interface Sci.*, 2002, **97**, 205–253.
- 4 D. Shukla and V. K. Tyagi, *J. Oleo Sci.*, 2006, **55**, 381–390.
- 5 R. Sharma, A. Kamal, M. Abdinejad, R. K. Mahajan and H.-B. Kraatz, *Adv. Colloid Interface Sci.*, 2017, **248**, 35–68.
- 6 E. Alami, G. Beinert, P. Marie and R. Zana, *Langmuir*, 1993, **9**, 1465–1467.
- 7 Z. Wang, Y. Li, X.-H. Dong, X. Yu, K. Guo, H. Su, K. Yue, C. Wesdemiotis, S. Z. D. Cheng and W.-B. Zhang, *Chem. Sci.*, 2013, **4**, 1345–1352.
- 8 K. Hamaguchi, R. Ichikawa, S. Kajiyama, S. Torii, Y. Hayashi, J. Kumaki, H. Katayama and T. Kato, *ACS Appl. Mater. Interfaces*, 2021, **13**, 20598–20605.
- 9 T. Nishioka, K. Kuroda, M. Akita and M. Yoshizawa, *Angew. Chem., Int. Ed.*, 2019, **58**, 6579–6583.
- 10 C. Bombelli, L. Giansanti, P. Luciani and G. Mancini, *Curr. Med. Chem.*, 2009, **16**, 171–183.
- 11 S. Mahajan and R. K. Mahajan, *Adv. Colloid Interface Sci.*, 2013, **199**, 1–14.
- 12 M. Rodrigues, A. C. Calpena, D. B. Amabilino, M. L. Garduño-Ramírez and L. Pérez-García, *J. Mater. Chem. B*, 2014, **2**, 5419–5429.
- 13 A. K. Singh, K. Achazi, S. Ehrmann, C. Böttcher, R. Haag and S. K. Sharma, *Polym. Chem.*, 2020, **11**, 6772–6782.
- 14 A. Mittal, F. Zabihi, F. Rancan, K. Achazi, C. Nie, A. Voggt, R. Haag and S. K. Sharma, *RSC Adv.*, 2022, **12**, 23566–23577.
- 15 M. C. Grenier, R. W. Davis, K. L. Wilson-Henjum, J. E. LaDow, J. W. Black, K. L. Caran, K. Seifert and K. P. C. Minbiole, *Bioorg. Med. Chem. Lett.*, 2012, **22**, 4055–4058.
- 16 A. Pinazo, M. A. Manresa, A. M. Marques, M. Bustelo, M. J. Espuny and L. Pérez, *Adv. Colloid Interface Sci.*, 2016, **228**, 17–39.
- 17 K. Taleb, M. Mohamed-Benkada, N. Benhamed, S. Saidi-Besbes, Y. Grohens and A. Derdour, *J. Mol. Liq.*, 2017, **241**, 81–90.
- 18 R. Qi, N. Zhang, P. Zhang, H. Zhao, J. Liu, J. Cui, J. Xiang, Y. Han, S. Wang and Y. Wang, *ACS Appl. Mater. Interfaces*, 2020, **12**, 17220–17229.
- 19 B. Brycki and A. Szulc, *J. Mol. Liq.*, 2021, **344**, 117686.
- 20 A. R. Ahmady, P. Hosseinzadeh, A. Solouk, S. Akbari, A. M. Szulc and B. E. Brycki, *Adv. Colloid Interface Sci.*, 2022, **299**, 102581.
- 21 C. Borde, V. Nardello, L. Wattebled, A. Laschewsky and J.-M. Aubry, *J. Phys. Org. Chem.*, 2008, **21**, 652–658.
- 22 M. Rodrigues, A. C. Calpena, D. B. Amabilino, D. Ramos-López, J. de Lapuente and L. Pérez-García, *RSC Adv.*, 2014, **4**, 9279–9287.
- 23 M. E. Alea-Reyes, A. González, A. C. Calpena, D. Ramos-López, J. de Lapuente and L. Pérez-García, *J. Colloid Interface Sci.*, 2017, **502**, 172–183.
- 24 S. Wang, X. Xin, H. Zhang, J. Shen, Y. Zheng, Z. Song and Y. Yang, *RSC Adv.*, 2016, **6**, 28156–28164.
- 25 F. Tao and S. L. Bernasek, *Chem. Rev.*, 2007, **107**, 1408–1453.
- 26 E. Yashima, N. Ousaka, D. Taura, K. Shimomura, T. Ikai and K. Maeda, *Chem. Rev.*, 2016, **116**, 13752–13990.
- 27 T. Shimizu, *Polym. J.*, 2003, **35**, 1–22.
- 28 A. D. Bond, *New J. Chem.*, 2004, **28**, 104–114.
- 29 Y. Li, P. Li, J. Wang, Y. Wang, H. Yan and R. K. Thomas, *Langmuir*, 2005, **21**, 6703–6706.
- 30 D. V. Perroni, C. M. Baez-Cotto, G. P. Sorenson and M. K. Mahanthappa, *J. Phys. Chem. Lett.*, 2015, **6**, 993–998.
- 31 S. Mantha, J. G. McDaniel, D. V. Perroni, M. K. Mahanthappa and A. Yethiraj, *J. Phys. Chem. B*, 2017, **121**, 565–576.



- 32 K. E. Jelfs, E. G. B. Eden, J. L. Culshaw, S. Shakespeare, E. O. Pyzer-Knapp, H. P. G. Thompson, J. Bacsá, G. M. Day, D. J. Adams and A. I. Cooper, *J. Am. Chem. Soc.*, 2013, **135**, 9307–9310.
- 33 Z. Xiong, J. Zhang, J. Z. Sun, H. Zhang and B. Z. Tang, *J. Am. Chem. Soc.*, 2023, **145**, 21104–22113.
- 34 R. Zana, *J. Colloid Interface Sci.*, 2002, **248**, 203–220.
- 35 M. Yamashina, H. Suzuki, N. Kishida, M. Yoshizawa and S. Toyota, *Angew. Chem., Int. Ed.*, 2021, **60**, 17915–17919.
- 36 H. Suzuki, Y. Akiyama, M. Yamashina, Y. Tanaka and S. Toyota, *Chem. – Eur. J.*, 2023, **29**, e202303017.
- 37 A. L. Clevenger, R. M. Stolley, J. Aderibigbe and J. Louie, *Chem. Rev.*, 2020, **120**, 6124–6196.
- 38 K. J. Sommers, M. E. Michaud, C. E. Hogue, A. M. Scharnow, L. E. Amoo, A. A. Petersen, R. G. Carden, K. P. C. Minbiole and W. M. Wuest, *ACS Infect. Dis.*, 2022, **8**, 387–397.
- 39 B. A. Pindzola, J. Jin and D. L. Gin, *J. Am. Chem. Soc.*, 2003, **125**, 2940–2949.
- 40 H. Oshiro, T. Kobayashi and T. Ichikawa, *Mol. Syst. Des. Eng.*, 2022, **7**, 1459–1466.
- 41 J.-H. Fuhrhop and T. Wang, *Chem. Rev.*, 2004, **104**, 2901–2937.

